

Unsupervised Learning Consensus Model for Dynamic Texture Videos Segmentation

Lazhar Khelifi, and Max Mignotte

Abstract—Dynamic texture (DT) segmentation, and video processing in general, is currently widely dominated by methods based on deep neural networks that require the deployment of a large number of layers. Although this parametric approach has shown superior performances for the dynamic texture segmentation, all current deep learning methods suffer from a significant main weakness related to the lack of a sufficient reference annotation to train models and to make them functional. In addition, the result of these methods can deteriorate significantly when the network is fed with images or video not similar (as regards, shape, texture, color, etc.) to the images previously included in the training dataset. This study explores the unsupervised segmentation approach that can be used in the absence of training data to segment new videos. In particular, it tackles the task of dynamic texture segmentation. By automatically assigning a single class label to each region or group, this task consists of clustering into groups complex phenomena and characteristics which are both spatially and temporally repetitive. We present an effective unsupervised learning consensus model for the segmentation of dynamic texture (ULCM). This model is designed to merge different segmentation maps that contain multiple and weak quality regions in order to achieve a more accurate final result of segmentation. The diverse labeling fields required for the combination process are obtained by a simplified grouping scheme applied to an input video (on the basis of a three orthogonal planes: xy , yt and xt). In the proposed model, the set of values of the requantized local binary patterns (LBP) histogram around the pixel to be classified are used as features which represent both the spatial and temporal information replicated in the video. Experiments conducted on the challenging SynthDB dataset show that, contrary to current dynamic texture segmentation approaches that either require parameter estimation or a training step, ULCM is significantly faster, easier to code, simple and has limited parameters. Further qualitative experiments based on the YUP++ dataset prove the efficiently and competitively of the ULCM.

Index Terms—Video processing, dynamic texture segmentation, consensus framework, unsupervised learning, optimization, global consistency error (GCE).

I. INTRODUCTION

DYNAMIC TEXTURE, or texture movie, combines texture in the spatial domain with motion (with some form of stationarity) in the temporal domain [1] (see Fig. 1). Consequently, dynamic texture segmentation can be very complex because this process requires to jointly analyze spatiotemporal data which can be very different in nature, just like the numerous dynamic scenes existing in the real world, such as; cloud, falling snow, flowing flag, swirl, smoke, etc. [2].

L. Khelifi and M. Mignotte are with Department of Computer Science and Operations Research, Montreal University, Montreal, Quebec, Canada (e-mail: khelifi@iro.umontreal.ca, mignotte@iro.umontreal.ca. (see <http://www.lazharkhelifi.com>)

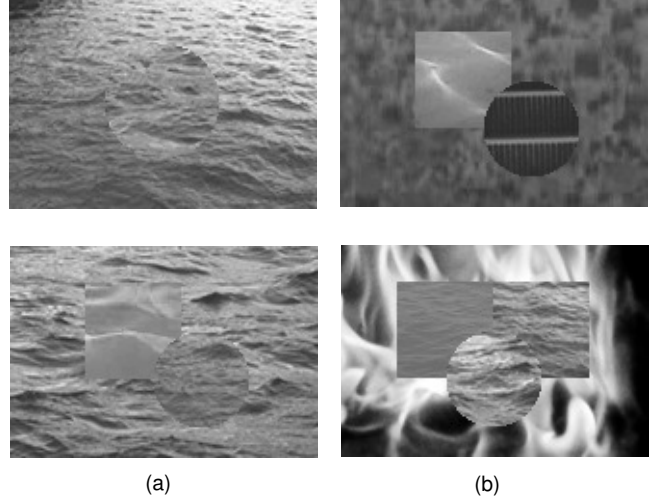


Fig. 1. Examples of DTs. (a) DTs are different regarding motion or displacement (i.e. in temporal mode), but similar in terms of appearance (i.e. in spatial mode) related mainly to texture. (b) DTs are different with respect to appearance, but similar in terms of motion ¹.

Recently, research on dynamic segmentation of textures has been of growing interest and has led to the development of interesting and varied methods. Doretto *et al.* [3] used spatio-temporal statistics and more precisely their dynamics over time with Gauss-Markov models [4] to segment a sequence of images into regions. A variational optimization framework was then used to infer the parameters of the model and to locate the boundary of each region. However, a limitation of this model is based on the assumption that regions vary slowly over time and also essentially according to the irradiance within each region. Vidal *et al.* [5], for their part, tackled this problem by first analyzing a generalized principal component analysis (GPCA) of the optical flow field generated from the video which was finally exploited to segment the spatiotemporal data by grouping pixels having similar trajectories in time. Nevertheless, as it was originally designed, this segmentation model is limited to only two classes. Chan *et al.* [6] proposed the mixture of dynamic textures (DTM) as an appropriate representation for both the dynamics and appearance of dynamic texture videos. In their model, the different parameters are learned using the expectation-maximization (EM) algorithm. Their work was extended in [8] by using the efficiency of the GPU computations to accelerate the segmentation process. Wattanachote *et al.* [9] presented a new and original

¹http://www.ee.oulu.fi/~gyzhao/research/dynamic_texture_recognition.htm

method of semi-automatic dynamic segmentation of textures by exploiting motion vectors generated from the model of Farnebäck² [10]. Nevertheless, an important constraint of this technique is that user interaction is still required to select the focus objects and to fine-tune the result to produce a high quality spatiotemporal segmentation map. Nguyen *et al.* [11] proposed a novel automatic feature selection dynamic mixture model (FSDTM) to solve the motion segmentation problem. The key strength of their approach is that it is totally unsupervised and does not require a set of training data having known classifications on which to fit the mixture model. In this approach, the expectation maximization (EM) method is exploited to estimate the parameters of the model of mixture in the maximum likelihood sense. However, the EM algorithm remains very sensitive to initial values, noise, outliers and to the shapes of the laws of distribution chosen a priori in the mixture model and has also the drawback of converging at local minima. An interesting (but partially supervised) approach combining a supervised learning method with a filter-based motion features has been introduced by Teney *et al.* [12].

Different from the existing methods, Cai *et al.* [13] have suggested a new dynamic texture methodology for ultrasound images. This model consists in a combination of surfacelet transform, parallel computing and HMT model. One advantage of this work is that makes it possible to build a model that both cover temporal and spatial information by considering simultaneously a sequence of images. Yousefi *et al.* [14] proposed an interesting non-parametric fully Bayesian approach for DT segmentation, built based on joining Dirichlet process mixture (DPM) with generative dynamic texture models (GDTMs). This method effectively eliminates the required information on the amount of textures and its initial partitioning. In [15] authors discussed three DT segmentation methods based on global spatiotemporal technique (contourlet transform), local spatiotemporal technique (local binary pattern) and optical flow. Their experimentation conducted through these individual techniques and also using certain combinations of them. Results showed that local binary pattern is simple to be implemented, less computationally complex and represents a suitable variant can be considered depending on the application at hand. However, optical flow technique is more computationally complex but still represents a natural way of motion detection. This study also showed the capability of contourlet transform in tracing smooth contours, especially, in case of images that contain natural DTs. Among the most recent work, one can cite the algorithm proposed by Andrearczyk *et al.* [16] in which a convolutional neural networks (CNNs) is applied on three orthogonal slices xt , xy and yt of an input video sequence. The major drawback in their approach is that the training of independent CNNs on three orthogonal planes, and the combination of their outputs makes the process more complex from a computational point of view while being also supervised. The major drawback of their approach is that the training of individual CNNs on three orthogonal

planes, as well as the combination of their outputs, render the entire procedure more computationally complex from a computational point of view while being also supervised.

Motivated by the above observations, we herein introduce a novel fusion model for dynamic texture segmentation called ULCM. Our model combines multiple and soft segmentation maps in order to obtain a more consistent and high-quality spatiotemporal segmentation result. These initial and weak partition maps are estimated from separate slices (or frames) of the video sequence and across the different axis of the data cube. In addition, in order to overcome the disadvantages of previous methods that often lead to complex estimation, optimization or combinatorial problems, we herein propose a simple energy-based model based on an efficient segmentation fusion criterion derived from the global consistency error (GCE). This metric of GCE is a perceptual measure that considers the inherently multi-scale property of any image partition (potentially qualified as a refinement of an existing segmentation) by quantifying the level of difference of two segmentation maps. Moreover, to efficiently optimizing our energy-based model, we introduce a modified local optimization scheme derived from the Iterative Conditional Mode method (ICM).

In summary, this study provides the following three main contributions:

- A new consensus model of unsupervised learning is proposed for the dynamic segmentation of textures. The developed model combines multiple and weak segmentation results to obtain a finer and more reliable segmentation of an input video.
- An energy function derived from the global coherence error (GCE) is proposed for the fusion process. The GCE measure is a perceptual criterion that considers the inherently multi-scaled nature of an image segmentation (by calculating the degree of refinement within two spatial segments).
- Extensive experiments on two reference datasets demonstrate the effectiveness of the proposed unsupervised method and its ability to achieve high quality segmentation results with clear boundaries.

The rest of the article is arranged as follows: First of all, we provide a brief definition of dynamic texture problem in section II. In Section III, we introduce the proposed ULCM fusion model. In Section IV, we present an experimental evaluation of the developed algorithm using synthetic and real video datasets. Finally, in Section V, we draw a conclusion.

II. DYNAMIC TEXTURE

While a variety of definitions of the dynamic texture has been suggested, this paper will use the definition first suggested by Chan *et al.* [6] who define it as a generative model for both the appearance (frame of video at time t), and the dynamics of video sequences (temporal evolution of the video), based on a linear dynamic system. Following this definition, a linear function of the current state vector, plus some observation noise, generally represents the appearance

²An algorithm for estimating dense optical flow based on modeling the neighborhoods of each pixel by quadratic polynomials.

of the image $y_t \in R^n$, while the state process evolving over time $x_t \in R^n$ (typically $n \ll m$) represents the dynamics. Mathematically, the equations of this system are defined as follows:

$$s(x) = \begin{cases} x_{t+1} = Ax_t + v_t \\ y_t = Cx_t + w_t \end{cases} \quad (1)$$

Where, the value of the present state x_t represents an essential element for the calculation of the next value of the state variable x_{t+1} , and also primordial for the prediction of the present value of the observation process y_t . $C \in R^m$ is a matrix that contains the main pieces of the video sequence, and the argument $A \in R^n$ represents state-transition matrix. The observation noise w_t is zero mean and Gaussian, with covariance R , that is, $w_t \sim N(0; R)$, where $R \in R^{m \times m}$. The driving noise process v_t is evenly distributed with zero mean and covariance Q , that is, $v_t \sim N(0; Q)$, where $Q \in R^{n \times n}$ is a positive-definite $n \times n$ matrix. It should be noted that a one-dimensional random trajectory in time is defined by each coordinate of the state vector x_t , and a value of weighted sum of random trajectories is then assigned to each pixel, where the coefficients of weights are included in the corresponding row of C . The dynamic texture is completely represented as a graphical model in Fig. 2.

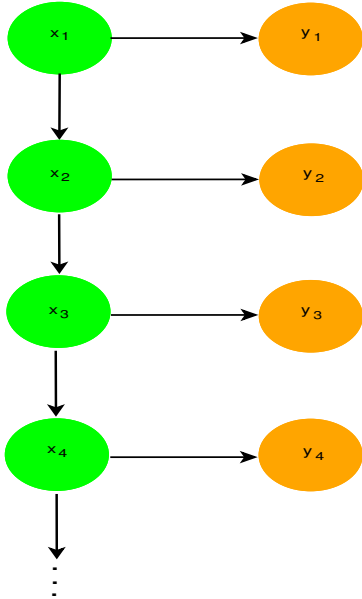


Fig. 2. Graphical model for dynamic texture DT. x_t and y_t represent the hidden state and the observed video image at the time t , respectively.

III. PROPOSED UNSUPERVISED LEARNING CONSENSUS MODEL (ULCM)

The method presented here is automatic, straightforward, and consists of five steps, as mentioned in our preliminary work [17]. In the first step of our method, an ensemble of images is typically obtained by slicing through the video cube (i.e. dynamic texture data). In the second stage, a procedure of feature extraction is proposed and performed for individual

images. In the third stage, for each extracted local histogram associated with each pixel, a variable stochastic dimensionality reduction method using different seeds is performed. Then, a clustering technique is employed to generate an ensemble of primary segmentations. Once these steps have been completed, in the fourth phase, an energy-based fusion scheme is performed across the ensemble of segmentation maps by iteratively optimizing a deterministic gradient-based optimization algorithm. The pseudo-code of the proposed method is outlined in Fig. 3.

A. Dynamic Texture Video Clipping

In order to fully benefit from the full complementarity of the three intrinsic (spatial and temporal) dimensions of our input video sequence V , and thus to more effectively represent each dynamic texture, we perform the following simple slicing operation: In addition to the classical slicing process; in which, in the xy spatial plane, we basically produce w equidistant slices that are equally separated in the t time plane from V corresponding to the w images contained in the video sequence, we have added two more clipping processes: First, in the xt time plane, we construct equidistant h slices (or frames) equally separated on the y axis. By this fact, the movement of a line of pixels in time over the length of the video is represented by a slice of the geometric plane xt . Second, in the time plane yt , we produce m equidistant frames equally spaced on the x axis. Concretely, the evolution of a column of pixels over time along the video sequence is represented by a slice of the yt plane. Finally, after this slicing stage, we get $h \times w \times m$ separate images in three sets (see Fig. 2).

B. LBP Representation

To more efficiently describe the texture, a feature extractor step is adopted by applying a Local binary pattern (LBP) operator to each previously generated frame. (see Fig. 4.(e)). The purpose of using the LBP operator is to describe the statistics of the micro-models within an image (i.e. a frame or slice in our case) by encoding the deviation between the central pixel value and its neighbor's values [18]. Formally, let q_c be the value of the center pixel c of a local neighborhood in a gray frame F . Suppose also that q_p ($p = 0, \dots, P-1$) represent the values of P equidistant pixels uniformly distributed around a circle with radius R forming a circularly symmetric set of neighbors. The coordinates of q_p are defined by $(R \sin(\frac{2\pi p}{P}), R \cos(\frac{2\pi p}{P}))$ in the case of coordinates of q_c are equal to $(0,0)$. Particularly, the values of neighbors that not falling precisely on pixels are obtained by bilinear interpolation. The LBP descriptor on this pixel (c) is given by:

$$LBP_{P,R} = \sum_{p=0}^{P-1} s(q_p - q_c) 2^p, \quad s(x) = \begin{cases} 1 & , x \geq 0 \\ 0 & , x < 0 \end{cases} \quad (2)$$

C. Segmentation Ensemble Generation

By adequately following the steps of our method, a projection process of all the pixels of each LBP generated image

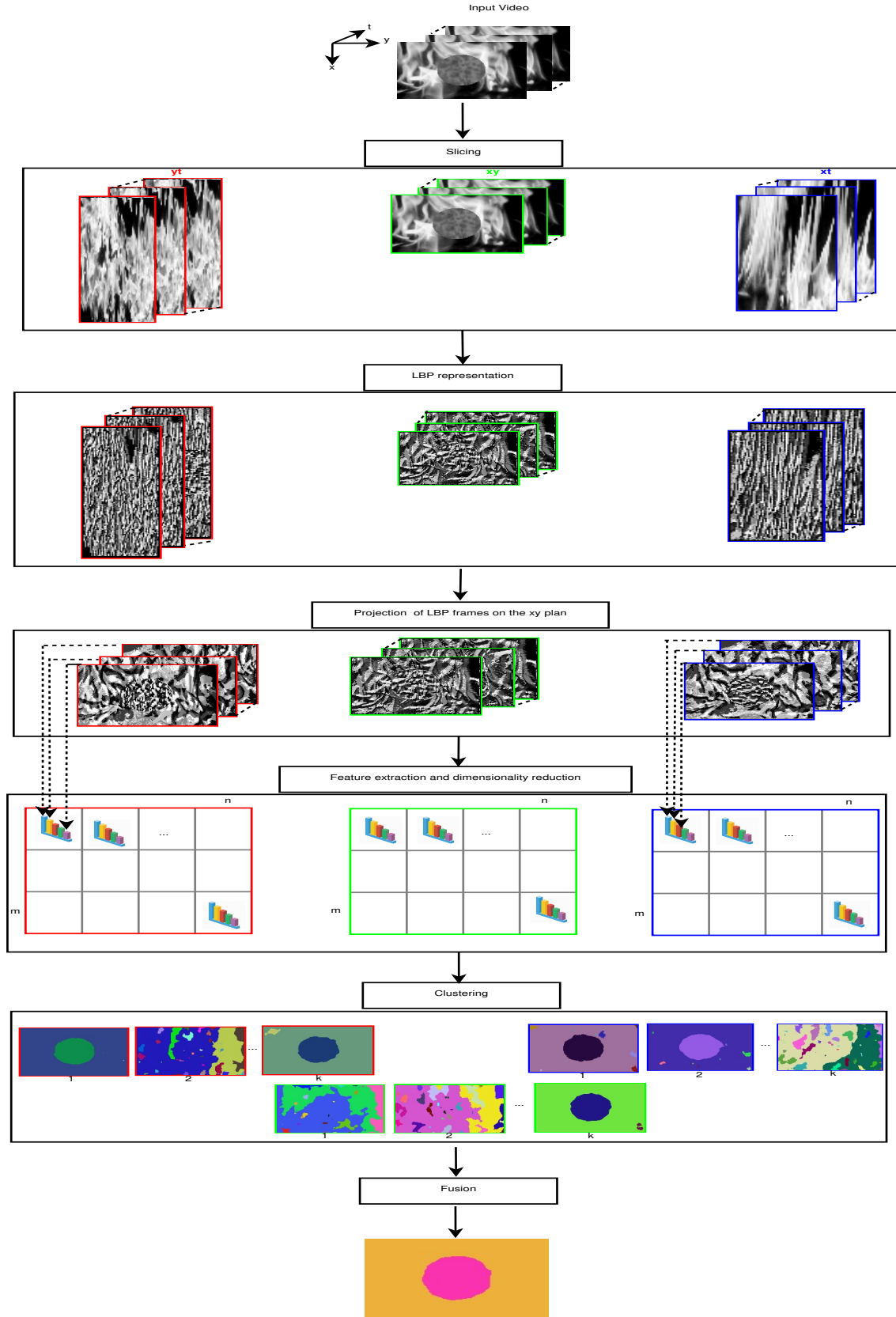


Fig. 3. Proposed system overview.

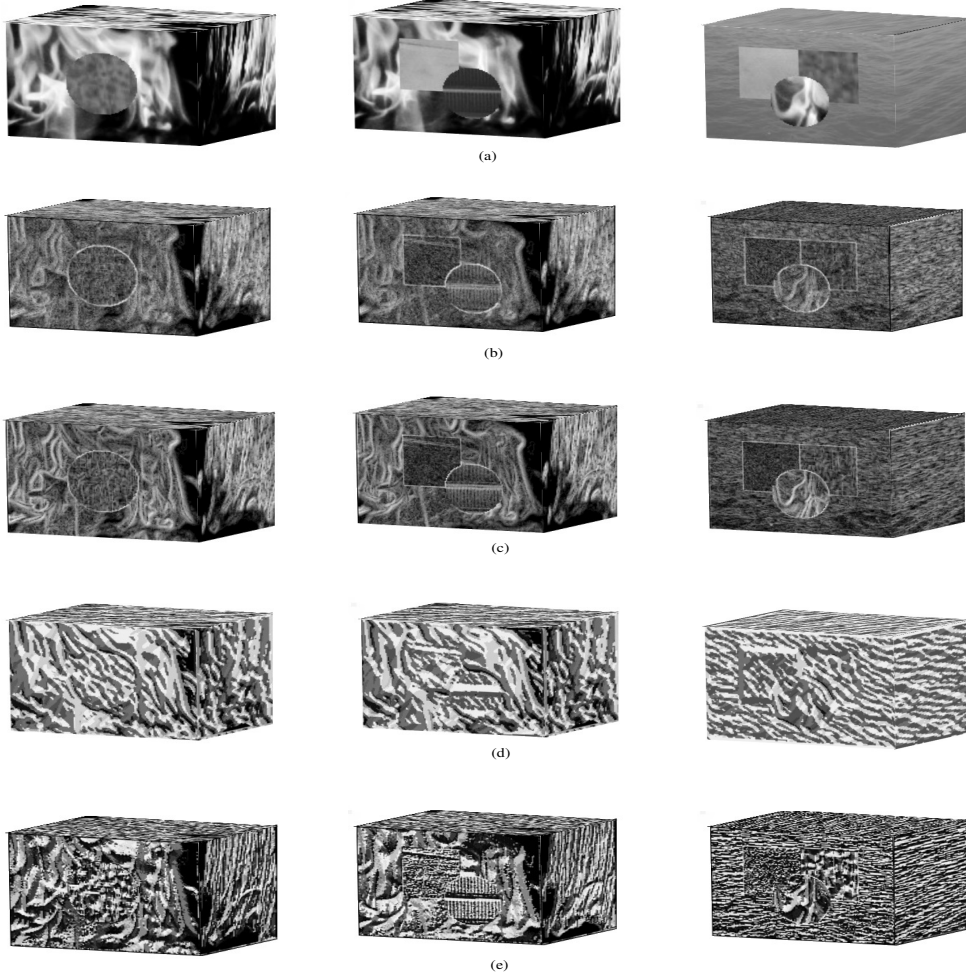


Fig. 4. Representation of the input video with different texture operator. (a) Original video, (b) Histogram of oriented gradients HOG, (c) Laplacian operator LAP, (d) local phase quantization LPQ, (e) local binary pattern LBP.

onto the xy plane is strongly required (cf. Fig. 3.(d)). Then, for each frame and for each pixel, we estimate, within an overlapping square of fixed size ($Nw = 7$ neighborhood centered around the pixel to be classified, a local requantized LBP histogram. In the next step, we concatenate all local histograms for the individual pixel $p_{(x,y)}^i$, each time t to finally create a high-dimensional feature histogram or vector (cf. Fig. 3.(e)). This high-dimensional histogram encloses a wide range of redundant features and masks the potential correlations between data which can make the interpretation of data much harder. For that reason, the dimensionality reduction methods [7] may be typically used here to avoid the lack of discrimination, often referred to the so-called *curse of dimensionality* problem³. In light of this situation, the original features should be preprocessed to simplify the high-dimensional histograms by transforming it into a low-dimensional structure. Also, it should be noted that, the precision of the segmentation must remain satisfactory while minimizing the amount of features to be handled and removing redundant information. In fact, dimensionality reduction is simply the process of projecting the n -dimensional data onto a subspace of a considerably less lower dimension (k) that represent a set of principal variables.

The commonly used approaches include principal component analysis (PCA) [19], multidimensional scaling (MDS) [20] and random projection (RP) [22] [21]. In our work we resort to the random projection (RP) for dimensionality reduction for two reasons. Firstly, RP is a much faster and less complex (linear complexity) compared to MDS and PCA (quadratic complexity). Secondly, RP has the ability to generate, by using different seeds, different (and low-dimensional) noisy projected data which will provide the necessary variability to our algorithm which then use it efficiently to obtain a final robust segmentation (this will be explicit in the following). Mathematically, in the random projection process, the original data matrix X [$n \times m$] is multiplied by a random projection matrix RP [$m \times k$] as follows:

$$X_{red} = \frac{1}{\sqrt{k}} \times X \times RP \quad (3)$$

where X_{red} is the result of the projection of the data onto a lower k dimensional subspace. Once the dimension reduction step is done, in order to generate groups, the clustering algorithm is applied to the different low-dimensional histograms⁴ (associated with the different seeds). Hence, we employ the well-known and useful k-means clustering technique [25]. We

have adopted this choice to assure a reduction in computing time and cost for this important step.

D. Fusion Using the Global Consistency Error Criterion

Once the set of segmentations is generated, we undertake to merge or fuse all these low quality segmentations into an energy-based fusion model according to the Global Coherence Error (GCE) criterion.

1) *Global Consistency Error Criterion*: The GCE criterion is a derivative of the so-called local refinement error (LRE), which attempts to quantify the similarity degree in terms of refinement, between two segments [26]. According to this perceptual criterion, segmentations are supposed to be consistent when they reflect the same image segmented at different levels of detail (or scale) [27] [28] or, in other words, when they represent a more or less detailed version of the same segmentation. Formally, let suppose that n is in the number of pixels within the frame F and let $\Phi_\mu = \{s_\mu^1, s_\mu^2, \dots, s_\mu^{nb_\mu}\}$ & $\Phi_\nu = \{s_\nu^1, s_\nu^2, \dots, s_\nu^{nb_\nu}\}$ be, two segmentation maps of the same frame to be compared, nb_μ being the number of segments in Φ_μ and nb_ν the number of segments in Φ_ν . Let now p_i be a particular pixel and the couple $(s_\mu^{<p_i>}, s_\nu^{<p_i>})$ be the two segments containing this pixel, respectively in Φ_μ and Φ_ν . The LRE on this pixel p_i is then formulated by:

$$\text{LRE}(s_\mu, s_\nu, p_i) = \frac{|s_\mu^{<p_i>} \setminus s_\nu^{<p_i>}|}{|s_\mu^{<p_i>}|} \quad (4)$$

where \setminus denotes the algebraic operator of difference and $|X|$ the cardinality of the set of pixels X . Particularly, a 1 value signifies that the two regions overlap, inconsistently. Contrarily, an error of 0 indicates that the pixel is practically in the refinement region. [29]. A good way to force all local refinements to go in the same direction is to make the LRE metric symmetric. Thereby, every LRE must be measured at least twice, once in each sense, and this simple strategy finally leads us to the so-called global coherence error (GCE):

$$\text{GCE}^*(\Phi_\mu, \Phi_\nu) = \frac{1}{2n} \left\{ \sum_{i=1}^n \text{LRE}(s_\mu, s_\nu, p_i) + \sum_{i=1}^n \text{LRE}(s_\nu, s_\mu, p_i) \right\} \quad (5)$$

The GCE^* value lies in the range $[0, 1]$. A distance of 0 indicates a high similarity (in terms of level of details) between the two segmentation maps Φ_μ and Φ_ν . While a distance of 1 expresses a poor consistency or correspondence between the two segmentation maps to be compared.

³The curse of dimensionality is a phenomenon that occurs during the analysis of data in high-dimensional spaces. The addition of dimensions extends the points, rendering high-dimensional data highly sparse and uniformly distributed [23]. This sparsity critical for any algorithm for which statistical significance is required. It is important to note that the organization and retrieval of data are often based on detecting areas where objects are clustered into groups with similar properties (i.e. similar pixels in our case); in high-dimensional data, however, all objects tend to be sparse and disparate in a different way.

⁴The size of the final feature vector is 20 times smaller compared to the size of the original high-dimensional vector.

2) *Combination Step*: Now suppose that $\{\Phi_k\}_{k \leq J} = \{\Phi_1, \Phi_2, \dots, \Phi_J\}$ represents the set of J different (weak) segmentation maps to be combined or fused (according to the GCE criterion). Let us recall that $J = 3K$, with K being the number of segmentation maps which are produced from each set of frames (cf Fig. 3.(f)). As already mentioned, our ultimate goal is to get the best possible segmentation map $\hat{\Phi}$ of the video sequence V from this set of multiple low-cost and weak segmentations. The fused segmentation result retains all the complementary and redundant information of those weak segmentations [24]. To estimate this refined segmentation result which in fact represents a consensus or a compromise between these multiple weak segmentations, an original and efficient energy-based model framework is now proposed to allow us to reconcile (or fuse) these segmentations. The main goal of this model is to provide a segmentation map solution as close-as-possible, based on the measured GCE^* -distance with respect to all other segmentations $\{\Phi_k\}_{k \leq J}$. In this energy-based framework, if Θ_n denotes the set of all feasible segmentations utilizing n pixels, the consensus segmentation $\hat{\Phi}_{\text{GCE}^*}$ (which is optimal according to the GCE^* criterion) is then directly given as the minimizer of the following cost functional $\overline{\text{GCE}^*}$:

$$\hat{\Phi}_{\text{GCE}^*} = \arg \min_{\Phi \in \Theta_n} \overline{\text{GCE}^*}(\Phi, \{\Phi_k\}_{k \leq J}) \quad (6)$$

Our fusion model is thus formulated as an optimization problem involving a highly nonlinear cost function. To optimize this nonlinear function [see Eq (6)], stochastic optimization approaches, for example the simulated annealing [31], the genetic algorithm [40] or the exploration/selection/estimation (ESE) procedure [30] may be successfully exploited. These optimizers are assured to find the exact solution, however, with the drawback of a very high-processing time. Another solution that we have followed in this study is a deterministic optimization scheme based on Besag's Iterative Conditional Mode (ICM) method [32] (which is actually also equivalent to a Gauss-Seidel based optimization scheme), where each label of a pixel is updated one at a time [33] [34]. In the present case, this algorithm has the benefit of being simple to implement while also being fast and efficient in terms of convergence.

IV. EXPERIMENTS AND DISCUSSIONS

A. Experimental Setup

Evaluation Datasets. We have evaluated our model quantitatively on SynthDB, a synthetic video texture database⁵ [6] containing 299 8-bit graylevel videos (image size is $160 \times 110 \times 60$ pixels). The video sequences are divided into three different sets (99 videos with 2 labels, 100 videos with 3 labels, and 100 videos with 4 labels), and a commonly ground truth model is provided for all the three sets. This data set is extremely challenging for two reasons: first, due to the fact that the videos are in grayscale, and also because the textures have a very similar static appearance. In addition, we have evaluated qualitatively the proposed method on the YUP++ [35] database.

TABLE I

PERFORMANCE OF THE ULCM METHOD COMPARED TO OTHER METHODS ON THE SYNTHDB DATASET (THE HIGHER VALUE OF PR INDEX, IS BETTER).

ALGORITHMS	PERFORMANCE (Avg. PR)		
	99 videos 2 labels	100 videos 3 labels	100 videos 4 labels
GPCA [5] in [38]	-0.52-	-0.48-	-0.53-
DTM [6]	-0.91-	-0.85-	-0.86-
DytexMixCS [6]	-0.92-	-0.83-	-0.84-
Color (Unsupervised) [12]	N/A	-0.60-	N/A
AR [41]	66	N/A	N/A
AR0 [41]	70	N/A	N/A
Color + motion (Unsupervised) [12]	N/A	-0.73-	N/A
Color + motion (Learned, logistic regression) [12]	N/A	-0.78-	N/A
Color + mouvement (Unsupervised) [12]	-0.71-	-0.61-	-0.61-
Color + HoME + mouvement (Unsupervised) [12]	-0.86-	-0.80-	-0.74-
Ising [41]	-0.88-	N/A	N/A
-ULCM-	-0.95-	-0.86-	-0.80-

TABLE II

PERFORMANCE OF THE PROPOSED METHOD USING DIFFERENT FUSION CRITERIA ON THE SYNTHDB DATASET (PR INDEX, HIGHER IS BETTER).

FUSION CRITERIA	PERFORMANCE (Avg. PR)		
	99 videos 2 labels	100 videos 3 labels	100 videos 4 labels
-F-measure-	0.937	0.756	0.710
-VoI-	0.947	0.823	0.763
-PRI-	0.919	0.743	0.710
-GCE-	0.953	0.855	0.796

TABLE III

PERFORMANCE OF THE ULCM METHOD USING DIFFERENT TEXTURE FEATURES ON THE SYNTHDB DATASET (PR INDEX, HIGHER IS BETTER).

FEATURES	PERFORMANCE (Avg. PR)		
	99 videos 2 labels	100 videos 3 labels	100 videos 4 labels
-LAP-	0.782	0.684	0.674
-HOG-	0.771	0.692	0.695
-LPQ-	0.696	0.610	0.572
-OLBP-	0.954	0.823	0.808
-VLBP-	0.760	0.659	0.686
-ELBP-	0.953	0.855	0.796

Evaluation Metric. We also rely on the probabilistic Rand (PR) index [36] for the evaluation of segmentation performance. This metric is widely used in the study of the performance of image (sequence) segmentation algorithms. More precisely, the PR index metric counts the number of pixel pairs with exactly the same labeling between two image segmentations to be measured. Mathematically, consider two valid label assignments, an automatic segmentation S_{aut} and

a manual segmentation (i.e., ground truth) S_{gt} of N pixels $P = p_1, p_2, \dots, p_i, \dots, p_N$ that attribute labels b_i and b'_i respectively to pixel p_i . The Rand index R can be given as the ratio of the number of pairs of pixels with a consistent label relationship in S_{aut} and S_{gt} . Therefore, the probabilistic rand index (PR) can be considered as follows:

$$R(S_{aut}, S_{gt}) = \frac{1}{C_N^2} \sum_{i,j;i < j}^n [I(b_i = b'_i \wedge b_j = b'_j) + I(b_i \neq b'_i \wedge b_j \neq b'_j)] \quad (7)$$

where C_N^2 is the number of possible unique pairs among N data points and I denotes the identity function. A “1” score signifies a good result, while a “0” score represents the worst possible segmentation.

B. Results and discussions

The performance of the suggested method is compared with the generalized principal component analysis (GPCA) [5], dynamic texture mixture model (DTM) [6], DytexMixCS [6], Ising [41], AR [41], AR0 [41] and others methods, proposed in [12], which are based on different types of features (including color, motion and movement) and metrics. Table I highlights that the proposed unsupervised method outperforms the other current state-of-the-art methods, even though our method has the advantage of not requiring any supervision and/or specific initialization step. As a result, we obtain an interesting PR score equals 0.953.

Additionally, to provide a qualitative comparison of the performance of the proposed method versus another set of methods, we present an example of an experiment in Fig. 5. In this experiment, our model is compared against the layered dynamic textures (LDT) [39], the supervised and unsupervised (based learning metric) approaches presented in [12] and the dynamic texture model (DTM)

⁵The synthetic video texture database is publicly accessible via this link: <http://www.svcl.ucsd.edu/projects/motiondytex/>

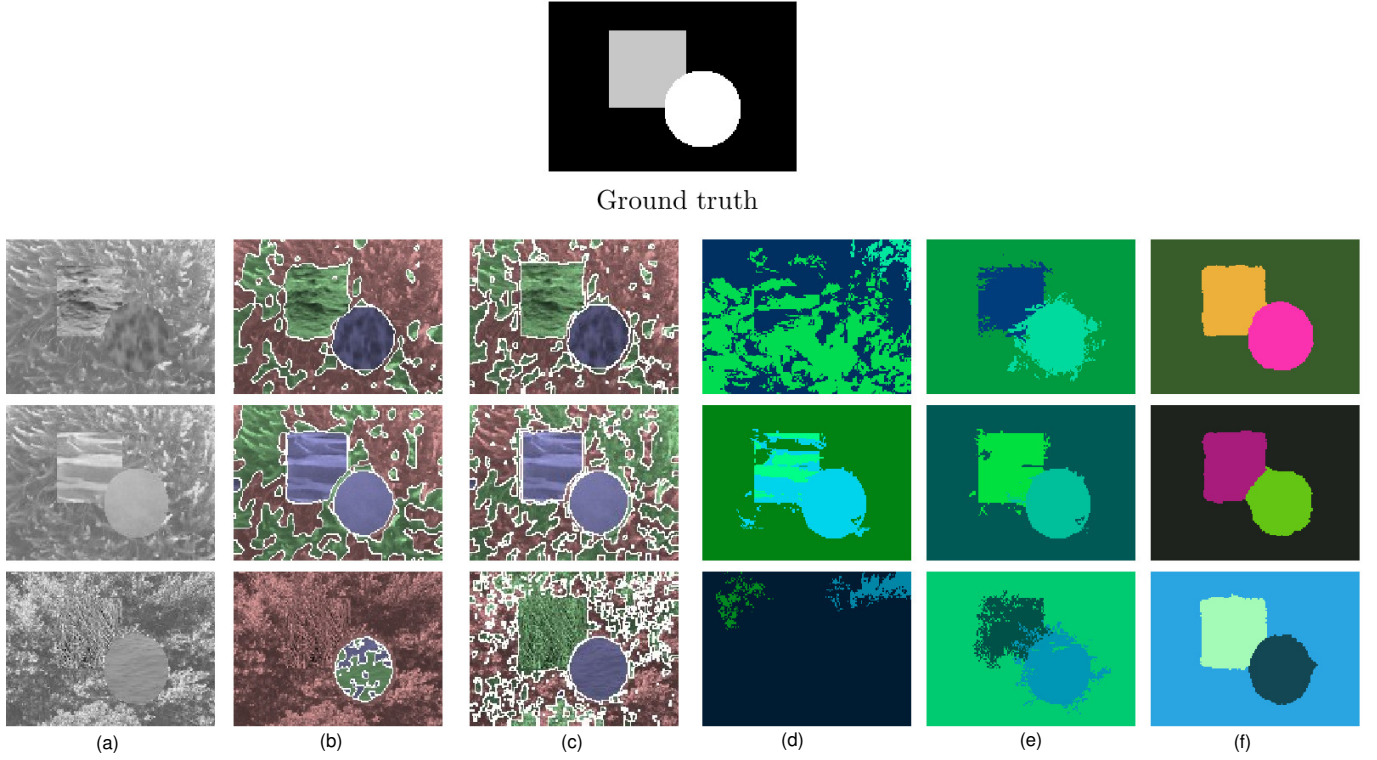


Fig. 5. Examples of segmentation results produced by the suggested method on three videos (with three labels)) of the SynthDB dataset [6] versus results of other algorithms. (a) Input video, (b) LDT with manual initialization [39], (c) DTM with contour initialization [6], (d) Color+motion Unsupervised [12] (f), Color+motion Learned [12], (e) Proposed method Unsupervised.

[6]. The result of the presented method, as illustrated in the sixth column, is significantly better as compared to other methods. In Fig. 6 we present additional segmentation results obtained from the SynthDB dataset based on our suggested method. Results on the complete dataset are available publicly on-line in the website of the corresponding author at the following [http](http://www-etud.iro.umontreal.ca/~khefilif/ResearchMaterial/consensus-video-seg.html) address: <http://www-etud.iro.umontreal.ca/~khefilif/ResearchMaterial/consensus-video-seg.html>. Besides the GCE criterion, We have also tested the effects of using different fusion criteria. Thus, in Table II, we report the performances yielded by our algorithm based on the following criteria:

- Probabilistic Rand Index (PRI), in which agreements and disagreements are weighted based on the probability of their occurring by chance [42].
- Variation of information (VoI), in which the information shared between two partitions is measured, in terms of the amount of information that is lost or gained in changing from one clustering to another [37].
- F-measure which is based on the combination of two complementary measures, namely precision (P) and recall (R) [37].

This test shows that the GCE is the most reliable criteria that yielding the best PR index. In contrast, the lower PR index is achieved based on the PRI criterion with values equal to 0.911 , 0.743 and 0.710, respectively, for videos with two, three and four labels. This significant superiority of the GCE criterion is due to its ability to take into account the

intrinsically multi-scale nature of image segmentation results. As another evaluation test, in Fig. 7 we present different results of segmentation related to three different videos obtained on the basis of these criteria. Indeed, compared to the PRI, the VOI and the F-measure based results, the GCE criterion (in (e)) carries out an improved qualitative results. This clearly shows the effectiveness of our choice to use this criterion.

Moreover, in table III, we outline the performance of the proposed method using different texture features including; Laplacian operator (LAP) histogram of oriented gradients (HOG), local phase quantization (LPQ), oriented local binary pattern (OLBP), extended local binary pattern (ELBP) and volume local binary pattern (VLBP). From this table we can conclude that OLBP and ELBP operator histogram are the features that yield the highest-scoring PR index. One reason for this good results is that OLBP feature combines together information regarding pixel intensity difference and texture orientation to capture the salient targets.

With the purpose of testing the robustness of the proposed technique against the variability of dynamic objects, we experiment it on the YUP++ database. Thus, in Fig. 8 we present different segmentation results for complex scenes with waving flags, waterfall and escalator.

Finally, in Fig.10 and Fig.11 we present a plot of the average PR obtained for each class label (of the SynthDB) and the computing time according to the dimension of the histogram of features (k). As can be seen from these figures, the competition time increases considerably as the histogram size increases, and the best average RP value (for the different

TABLE IV
COMPLEXITY OF THE DIFFERENCE STEPS OF THE ULCM

Steps	Complexity
LBP representation	$O(m \times n \times l \times r \times 3)$
Dimensionality reduction	$O(m \times n \times l \times k)$
Clustering (K-means)	$O(N \times C \times Iter \times dim)$
Fusion	$O(Nbreg \times p)$

label categories) is obtained with a value of histogram size in the range of [80..120].

In summary, our method has the merit of being simple in terms of implementation and numerical computation, totally unsupervised while being efficient compared to others computationally demanding and complex video segmentation models that exist in the published literature. In particular, compared to deep learning based models that require a highly experienced and professional work to build a large dataset of images specifically annotated for each object type or class, our proposed model does not require any human annotations. In addition, our model remains widely perfectible; either by adding other weak segmentations (to be combined) using other interesting (and possibly complementary) features or by using a more efficient fusion criterion or distance in our energy-based fusion framework.

C. Algorithm complexity

Table IV shows in detail the complexity of the main steps of the proposed algorithm. Thus, the LBP representation step is characterized by a complexity time of $O(m \times n \times l \times r \times 3)$, where m , n , l and r are height, width, number of frames in the video, number of neighbor points to compute the center pixel, respectively. Here, the multiplication by 3 is related to our choice in using simultaneously the three plane xy , yt and xt . The complexity of the dimensionality reduction step is equal to $O(m \times n \times l \times k)$, where k denotes the dimension of the histogram related to each pixel. Moreover, the K-means clustering step is distinguished by a complexity of $O(N \times C \times Iter \times dim)$, where N , C , $Iter$ and dim are the number of points of each cluster, the number of clusters, the number of iterations and the dimension of each point to be classified, respectively. The last step of fusion is characterized by a complexity time of $O(Nbreg \times p)$, where p is the pixel number within the image and $Nbreg$ represents the number of regions existing in the set of segmentations (generated by k-means).

V. CONCLUSION

We have presented a new approach to segment video with dynamic textures. By combining multiple rough (low-quality) region-based segmentations of a video and using a new geometric criterion, we demonstrated that it is possible to achieve a more accurate final segmentation result. Experiments show that our model, while being simple, fully unsupervised, fast and perfectible, is comparable to the state-of-the-art methods

using supervised or semi-automatic strategy and even better than those relying on unsupervised approaches. A potential extension of this approach is to incorporate several types of features with the Local Binary Pattern (LBP) to better describe the dynamic texture. Another possible extension of this work is to combine other possible criteria (variation of information, F-measure and probabilistic rand index) to achieve a more reliable result. It is important to mention that the proposed model is adapted to be implemented in parallel or to take full advantage of GPU systems that allow different types of features or criteria to be processed simultaneously.

REFERENCES

- [1] F. Hajati, M. Tavakolian, S. Gheisari, Y. Gao, and A. S. Mian, "Dynamic Texture Comparison Using Derivative Sparse Representation: Application to Video-Based Face Recognition," *IEEE Transactions on Human-Machine Systems*, vol. 47, no. 6, pp. 970–982, 2017.
- [2] J. Chen, G. Zhao, M. Salo, E. Rahtu, and M. Pietikainen, "Automatic Dynamic Texture Segmentation Using Local Descriptors and Optical Flow," *IEEE Transactions on Image Processing*, vol. 22, no. 1, pp. 326–339, 2013.
- [3] G. Doretto, D. Cremers, P. Favaro, and S. Soatto, "Dynamic texture segmentation," in *Proc. 9th IEEE International Conference on Computer Vision (ICCV)*, vol. 2, pp. 1236–1242, Oct. 2003.
- [4] J. Sun, H. Zhu, Z. Xu, and C. Han, "Poisson image fusion based on Markov random field fusion model," *Information Fusion*, vol. 14, num. 3, pp. 241–254, 2013.
- [5] R. Vidal and A. Ravichandran, "Optical flow estimation and segmentation of multiple moving dynamic textures," in *Proc. IEEE Computer Society Conference on Computer Vision and Pattern Recognition (CVPR)*, 2005, vol. 2, pp. 516–521.
- [6] A. B. Chan and N. Vasconcelos, "Modeling clustering and segmenting video with mixtures of dynamic textures," *IEEE Transactions on Pattern Analysis and Machine Intelligence*, vol. 30, no. 5, pp. 909–926, May 2008.
- [7] S. Ayesha, M. K. Hanif, and R. Talib, "Overview and comparative study of dimensionality reduction techniques for high dimensional data," *Information Fusion*, vol. 59, no. 3, pp. 44–58, 2020.
- [8] F. G. Fernandez, M. E. Buemi, J. M. Rodriguez and J. C. Jacobo-Berlles, "Performance of dynamic texture segmentation using GPU," *J Real-Time Image Proc.*, vol. 11, pp. 1–9, 2016.
- [9] K. Wattanachote and T. K. Shih, "Automatic Dynamic Texture Transformation Based on a New Motion Coherence Metric," *IEEE Transactions on Circuits and Systems for Video Technology*, vol. 26, no. 10, pp. 1805–1820, 2016.
- [10] G. Farnebäck, "Two-frame motion estimation based on polynomial expansion," in *Image Analysis (Lecture Notes in Computer Science)*, vol. 2749. Berlin, Germany: Springer-Verlag, 2003, pp. 363–370.
- [11] T. M. Nguyen and Q. J. Wu, "An unsupervised feature selection dynamic mixture model for motion segmentation," *IEEE Transactions on Image Processing*, vol. 23, no. 3, pp. 1210–1225, 2014.
- [12] D. Teney, M. Brown, D. Kit, and P. Hall, "Learning similarity metrics for dynamic scene segmentation," in *Proc. IEEE Computer Society Conference on Computer Vision and Pattern Recognition (CVPR)*, 2015, pp. 2084–2093.
- [13] B. Cai, W. Ye, and J. Zhao, "A dynamic texture based segmentation method for ultrasound images with Surfacelet, HMT and parallel computing," *Multimed Tools Appl*, vol. 78, no. 5, pp. 5381–5401, 2019.
- [14] S. Yousefi, M. T. M. Shalmani, and A. B. Chan, "A Fully Bayesian Infinite Generative Model for Dynamic Texture Segmentation," *abs/1901.03968/abs/1901.03968*, pp. 1–38, 2019.
- [15] S. Paygude and V. Vyas, "Dynamic Texture Segmentation Approaches for Natural and Manmade Cases: Survey and Experimentation," *Arch. Computat. Methods. Eng.*, pp. 1–13, 2018.
- [16] V. Andrearczyk and P. F. Whelan, "Convolutional Neural Network on Three Orthogonal Planes for Dynamic Texture Classification," <http://arxiv.org/abs/1703.05530>, pp. 1–19, 2017.
- [17] L. Khelifi and M. Mignotte, "A Consensus Framework for Segmenting Video with Dynamic Textures," in *Proc. 15th IEEE International Conference on Advanced Video and Signal Based Surveillance (AVSS)*, 2018, pp. 1–6.

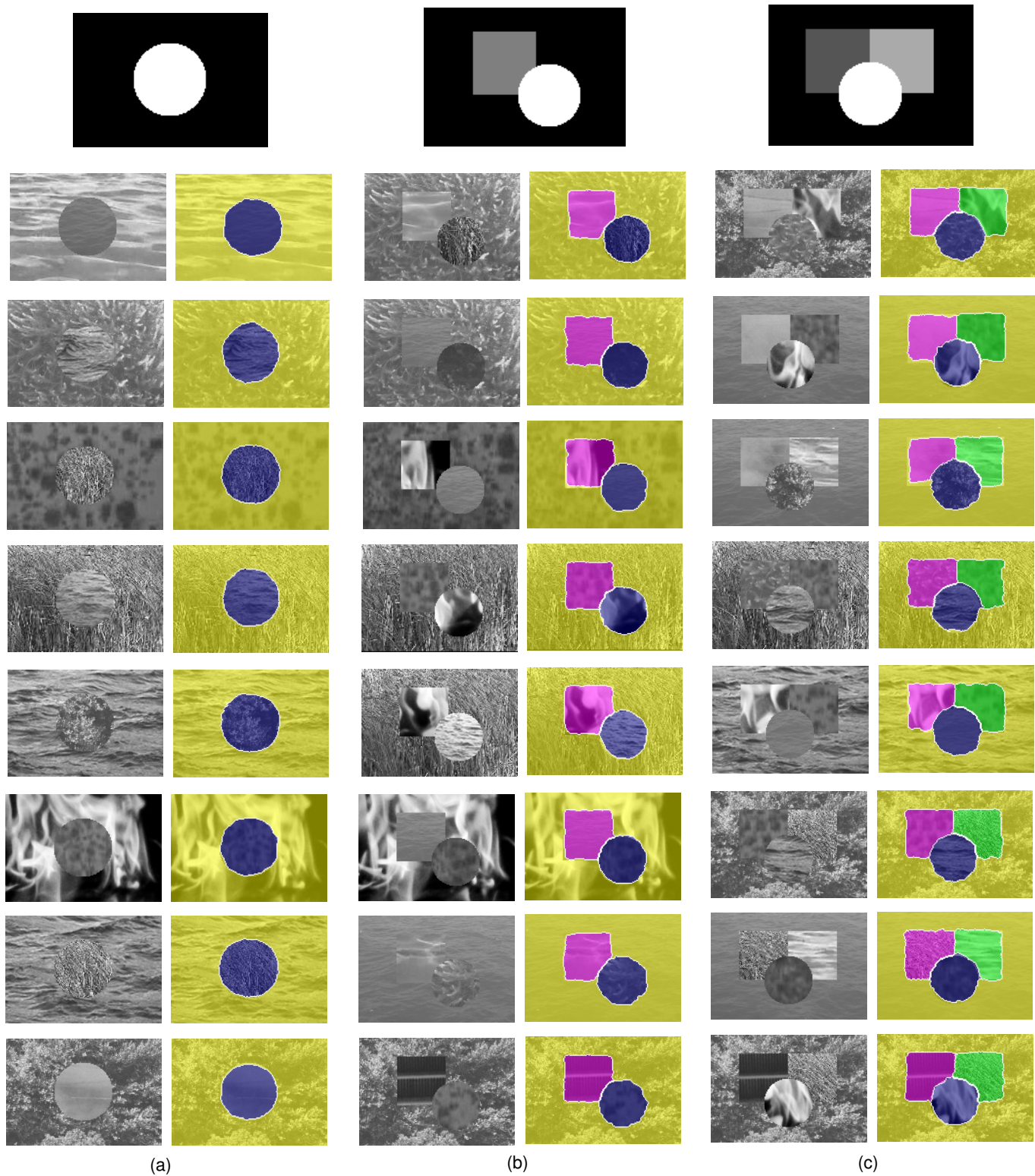


Fig. 6. More segmentation results achieved from the SynthDB dataset. (a) one labels, (b) two labels and (c) three labels.

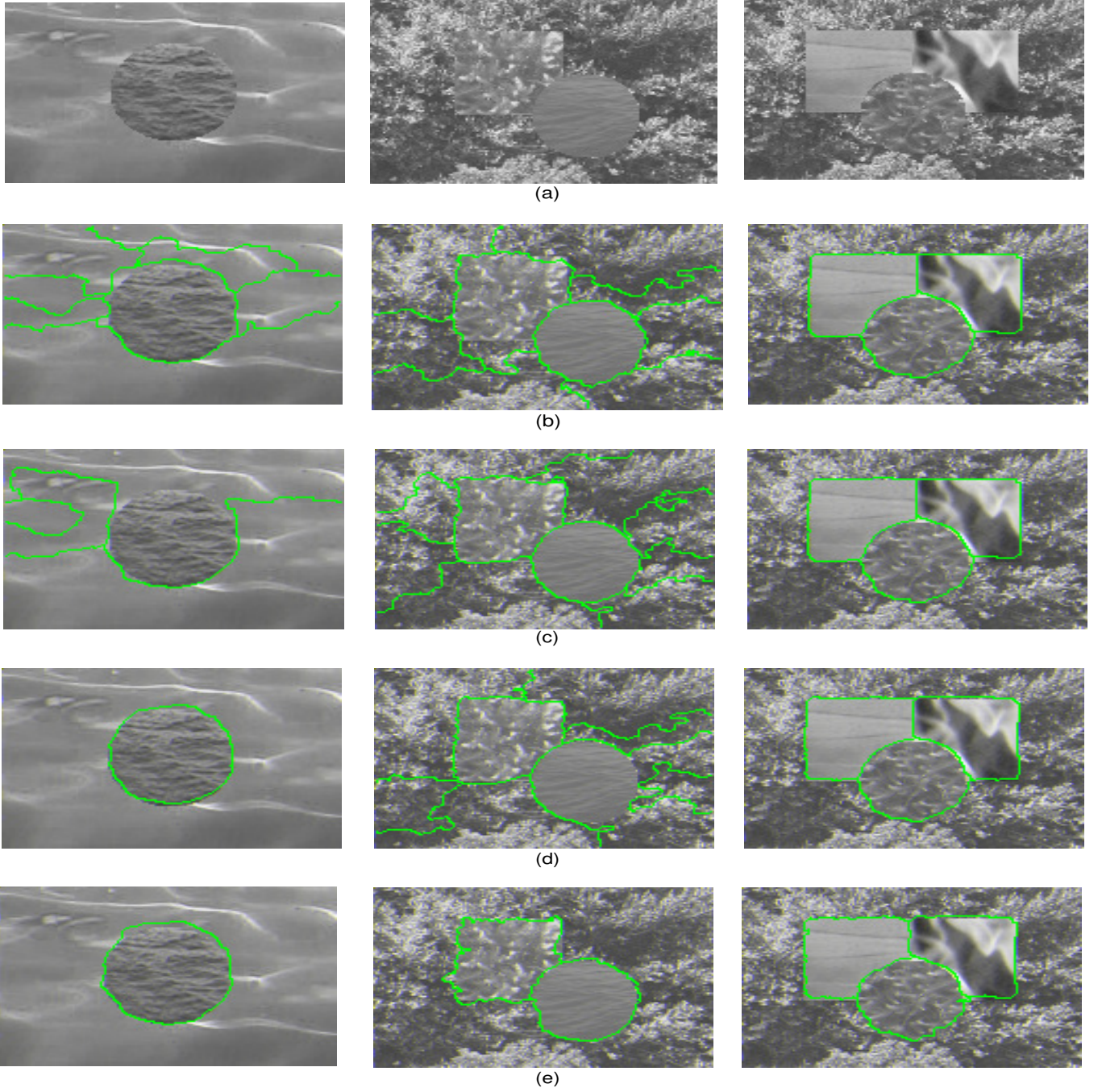


Fig. 7. Examples of segmentation results (generated by the proposed ULCM) of three videos based on different fusion criteria. (a) first frame of the video, (b) PRI, (c) VoI, (d) F-measure and (e) GCE.

- [18] T. Ojala and M. Pietikäinen and T. Mäenpää, "Multiresolution Gray-Scale and Rotation Invariant Texture Classification with Local Binary Patterns," *IEEE Transactions on Pattern Analysis and Machine Intelligence*, vol. 24, no. 7, pp. 971–987, 2002.
- [19] B. Lavanya and H. H. Inbarani, "A novel hybrid approach based on principal component analysis and tolerance rough similarity for face identification," *Neural Comput and Applic*, vol. 29, no. 8, pp. 289–299, 2018.
- [20] R. Marion, A. Bibal and B. Frnay, "BIR: A method for selecting the best interpretable multidimensional scaling rotation using external variables," *Neurocomputing*, vol. 342, pp. 83–96, 2019.
- [21] Q. Wang, J. Wan, F. Nie, B. Liu, C. Yan and X. Li, "Hierarchical Feature Selection for Random Projection," *IEEE Transactions on Neural Networks and Learning Systems*, vol. 30, no. 5, pp. 1581–1586, 2019.
- [22] B. Ella and M. Heikki, "Random Projection in Dimensionality Reduction: Applications to Image and Text Data," in *Proc. of the Seventh ACM International Conference on Knowledge Discovery and Data Mining (SIGKDD)*, 2001, pp. 245–250.
- [23] E. Debie and K. Shafi, "Implications of the curse of dimensionality for supervised learning classifier systems: theoretical and empirical analyses," *Pattern Analysis and Applications*, vol. 22, no. 2, pp. 519–536, May, 2019.
- [24] B. Meher, S. Agrawal, R. Panda, and A. Abraham, "A survey on region based image fusion methods," *Information Fusion*, vol. 48, pp. 119–132, 2019.
- [25] S. P. Lloyd, "Least squares quantization in PCM," *IEEE Transactions on Information Theory*, vol. 28, no. 2, pp. 129–136, 1982.
- [26] L. Khelifi and M. Mignotte, "A novel fusion approach based on the

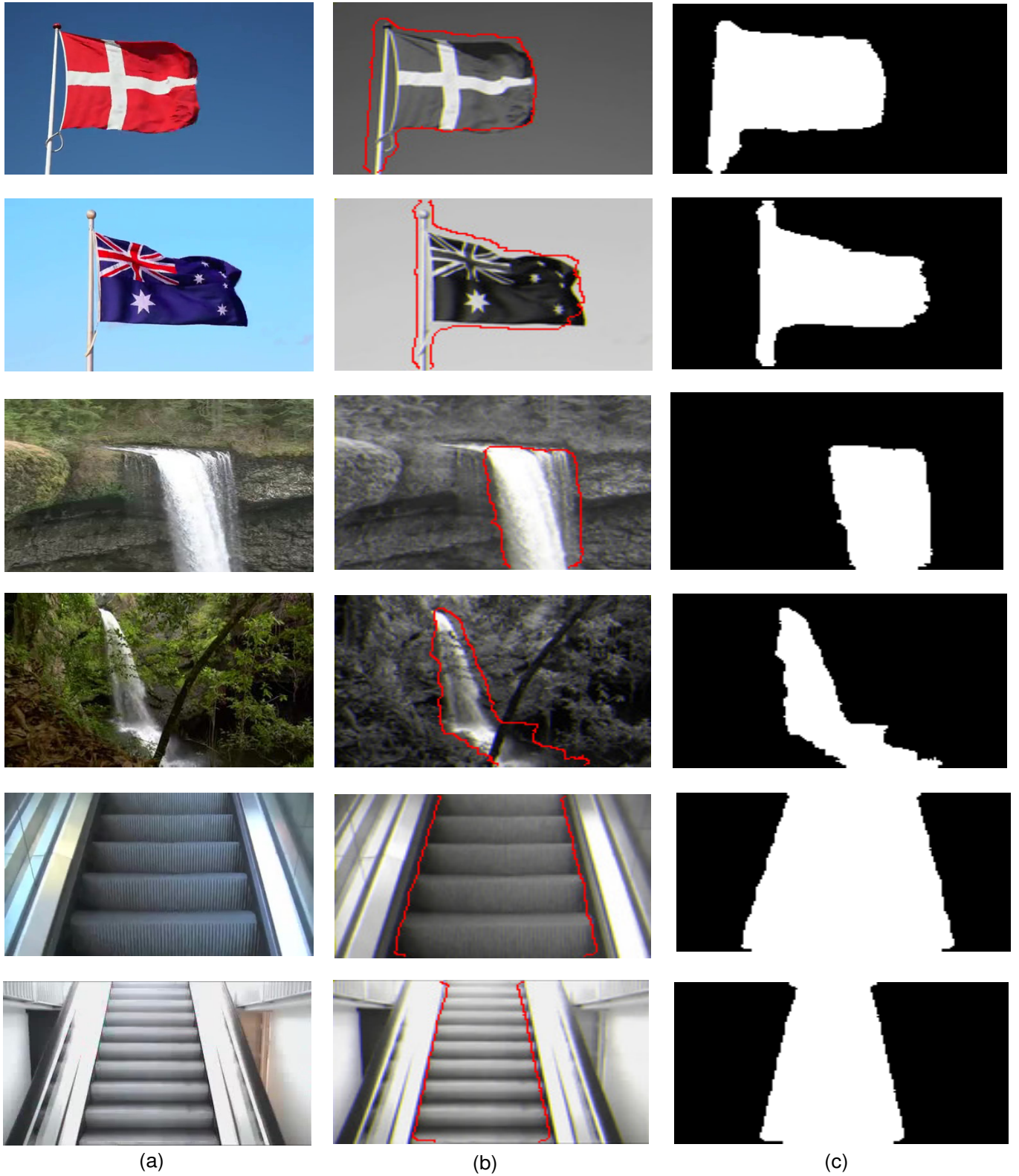


Fig. 8. Dynamic textures segmentation examples of YUP++ database (WavingFlags, Waterfall and Escalator): (a) images, (b) Segmented contours, (c) Segmented masks.

global consistency criterion to fusing multiple segmentations,” *IEEE Transactions on Systems, Man, and Cybernetics: Systems*, vol. 47, no. 9, pp. 2489–2502, September 2017.

[27] A. Y. Yang, J. Wright, S. Sastry, and Y. Ma, “Unsupervised segmentation

of natural images via lossy data compression,” *Computer Vision and Image Understanding*, vol. 110, no. 2, pp. 212–225, May 2008.

[28] L. Khelifi and M. Mignotte, “GCE-based model for the fusion of multiples color image segmentations,” in *Proc. 23rd IEEE International*

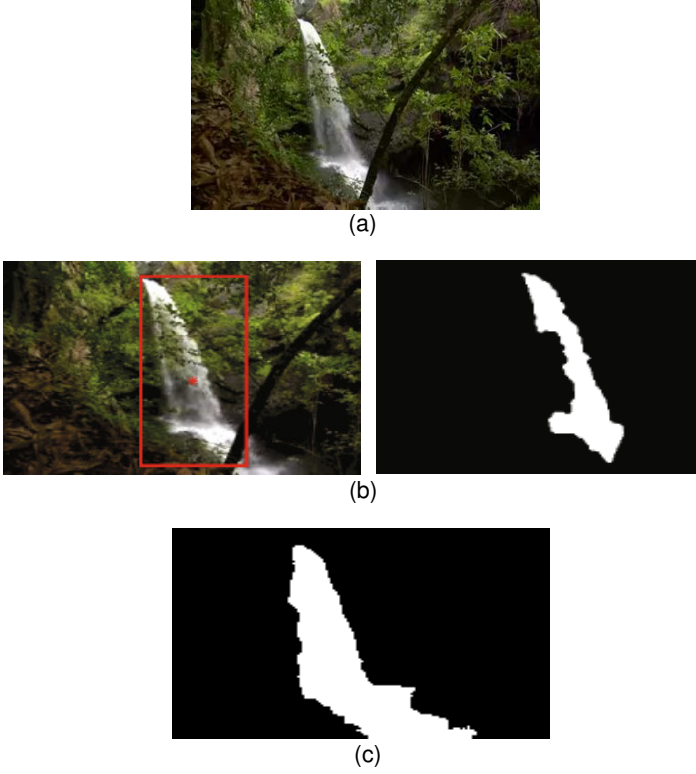


Fig. 9. An example of segmentation result obtained by our proposed method (without an initialization step) from the YUP++ dataset compared to ADAC Algorithm [35] (with an initialization step). (a) input video, (b) ADAC , (c) segmentation result based on our method.

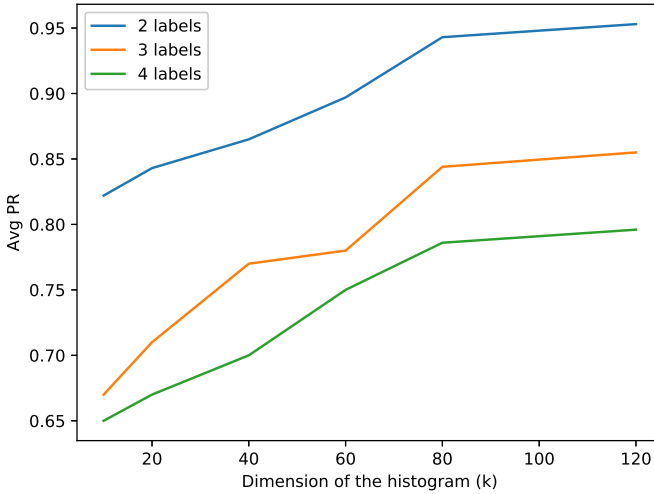


Fig. 10. Plot of the average PR obtained for each class label (of the SynthDB) as a function of the dimension of the histogram of features (k).

Conference on Image Processing (ICIP), 2016, pp. 2574–2578.

- [29] D. Martin, C. Fowlkes, D. Tal, and J. Malik, “A database of human segmented natural images and its application to evaluating segmentation algorithms and measuring ecological statistics,” in *Proc. 8th International Conference on Computer Vision (ICCV)*, vol. 2, July 2001, pp. 416–423.
- [30] F. Destremes, M. Mignotte, and J.-F. Angers, “A stochastic method for Bayesian estimation of hidden Markov models with application to a color model,” *IEEE Transactions on Image Processing*, vol. 14, no. 8,

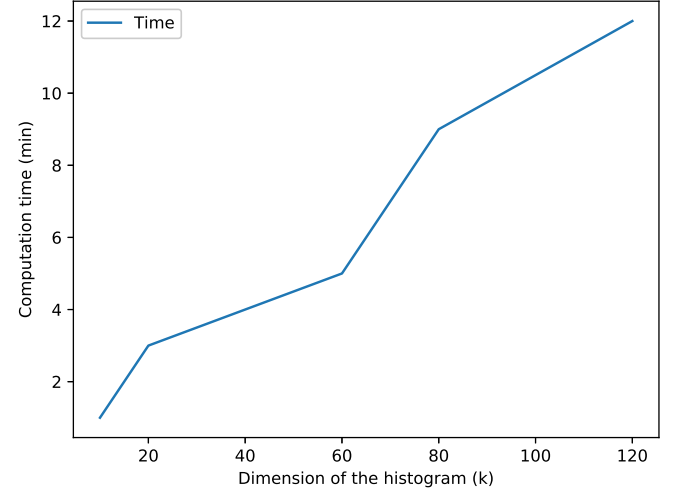


Fig. 11. Plot of the computing time as a function of the dimension of the histogram of features (k).

- pp. 1096–1108, 2005.
- [31] L. Khelifi, I. Zidi, K. Zidi, and K. Ghedira, “A hybrid approach based on multi-objective simulated annealing and tabu search to solve the dynamic dial a ride problem,” in *Proc. of the International Conference on Advanced Logistics and Transport (ICALT)*, 2013, pp. 227–232.
- [32] J. Besag, “On the statistical analysis of dirty pictures,” *Journal of the Royal Statistical Society*, vol. 48, no. 3, pp. 259–302, 1986.
- [33] L. Khelifi and M. Mignotte, “Semantic image segmentation using the ICM algorithm,” in *Proc. 24th IEEE International Conference on Image Processing (ICIP)*, Beijing, China, 2017.
- [34] L. Khelifi and M. Mignotte, “MC-SSM: Nonparametric Semantic Image Segmentation With the ICM Algorithm,” *IEEE Transactions on Multimedia*, vol. 21, no. 8, pp. 1946–1959, 2019.
- [35] I. Bida and S. Aouat, “Dynamic Textures Segmentation and Tracking Using Optical Flow and Active Contours,” *Information Systems and Technologies to Support Learning*, editor: A. Rocha and M. Serrhini, pp. 694–704, 2019.
- [36] R. Unnikrishnan, C. Pantofaru, and M. Hebert, “A measure for objective evaluation of image segmentation algorithms,” in *Proc. IEEE Computer Society Conference on Computer Vision and Pattern Recognition (CVPR)*, vol. 3, Jun. 2005, pp. 34–41.
- [37] L. Khelifi, M. Mignotte, “EFA-BMFM: A multi-criteria framework for the fusion of colour image segmentation,” *Information Fusion*, vol. 38, pp. 104–121, 2017.
- [38] T. M. Nguyen and Q. J. Wu, “A Consensus Model for Motion Segmentation in Dynamic Scenes,” *IEEE Transactions on Circuits and Systems for Video Technology*, vol. 26, no. 12, pp. 2240–2249, 2016.
- [39] A. B. Chan and N. Vasconcelos, “Layered dynamic textures,” *IEEE Transactions on Pattern Analysis and Machine Intelligence*, vol. 31, no. 10, pp. 1862–1879, Oct. 2009.
- [40] M. Mignotte, C. Collet, P. Perez, and P. Bouthemy, “Hybrid genetic optimization and statistical model-based approach for the classification of shadow shapes in sonar imagery,” *IEEE Transactions on Pattern Analysis and Machine Intelligence*, vol. 22, no. 2, pp. 129–141, 2000.
- [41] A. Ghoreyshi and R. Vidal, “Segmenting Dynamic Textures with Ising Descriptors, ARX Models and Level Sets,” in *Proc. European Conf. Computer Vision Dynamical Vision Workshop*, 2006.
- [42] C. Carpineto, and G. Romano, “Consensus clustering based on a new probabilistic rand index with application to subtopic retrieval,” *IEEE Transactions on Pattern Analysis and Machine Intelligence*, vol. 34, no. 12, pp. 2315–2326, 2012.